Universitetet i Stavanger

FACULTY OF SCIENCE AND TECHNOLOGY

MASTER THESIS

Study program/specialization: Master of Science in Drilling and Well Engineering	Spring 2020 Master Thesis
Author: Robert Michel Rosero Velasco	_____ (Author's signature)

Supervisor(s):
Dr. Mahmoud Khalifeh
Eng. Katherine Beltrán

Title of master's thesis:
Wall Temperature Analyses of Sandwiches Sections Using Infrared Thermography to Evaluate Micro-Annuli size

Credits: 30 ECTS

Keywords: Micro-annulus Surface temperature Inlet/Outlet temperature Flow channel rate Leakage path	Number of pages: XIII + 27 + supplemental material/other:10 Stavanger, 15th July 2020

Wall Temperature Analyses of Sandwiches Sections Using Infrared Thermography to Evaluate Micro-annuli size

By

Robert Michel Rosero Velasco

Master Thesis

Presented to the Faculty of Science and Technology

The University of Stavanger

THE UNIVERSITY OF STAVANGER

JULY 2020

Acknowledgement

I would like to thank NORCE for giving me the opportunity to use its facilities and be able to learn more about the topic thesis I decided to choose for my graduate program. Also, a special thanks to Katherine Beltrán and Steinar Kragset, who shared their experience knowledge with me on the subject and constant support.

I would like to thank the University of Stavanger who has been the institution where I have acquired the academic knowledge from during the last two years. A special thanks to my faculty supervisor, Mahmoud Khalifeh, who guided me throughout the project and gave me assistance for the improvement of the thesis outcome.

I would also like to thank my parents for helping me to see the world from a different perspective by encouraging me to study abroad. Thanks to this experience, I have been able to expand my mind and get out of my comfort zone to become a better person first, and then a better professional.

Finally, I would like to thank my entire family for all the constant support I have received throughout the years I have lived abroad because I would not have been able to overcome the challenges and obstacles I faced during the hard times to be where I am now, if it wasn't for them.

Abstract

This study mainly focuses on the detection and characterization of micro-annuli at the interface of cement and casing, usually caused by changes in pressure, temperature, or volume change of zonal isolation material. For the purposes of this study, leakage channel measurements of two pipes and the Infrared Thermography technique are analyzed to understand the size and shape of this gap.

To analyze the potential flow through the fluid migration leakage path, the assumption of "more than half full pipe flow" was used to estimate the flow rates for different channel heights using the Darcy-Weisbach and the Manning's equations. For the Manning's equation, initially a cast-iron channel surface was assumed and then a corrugated metal channel surface to assess the effect of friction losses.

The study shows that using the infrared thermography method has potential to characterize the leakage paths in sandwich casing sections. From the experiments, an anomaly was observed in a section of the investigated set-up (section C6), and after evaluation it was identified that the channel along this section was not uniform, and that the micro-annulus was not homogeneous. Investigating another section of the set-up (section A2), it did not show a visible anomaly or irregularity, and after analysis, it was concluded that the channel along this section was uniform, and that the micro-annulus was homogeneous.

The study also shows that the estimated leakage rates in section A2 using the Manning's equation for a corrugated metal channel surface are more accurate because of the uniformity of the channel, which is consistent with the results obtained using the infrared thermography cameras.

Acronyms

P &A- Plug and Abandonment

NORCE – Norwegian Research Centre

UiS – University of Stavanger

CBL – Cement Bond Log

Cw – Specific heat of water

Rh – Hydraulic radius

Dh – Hydraulic diameter

Ɵ - Sector angle

P – Wetted perimeter

n = Manning roughness coefficient value

S – friction slope of the channel

T surface middle – Surface temperature of pipe at half-length

Tin – Inlet temperature of the fluid

Tout – Outlet temperature of the fluid

List of Contents

List of Figures

List of Tables

1. Introduction

The infrared thermography method is an experimental technique used for detection of surface or near subsurface cracks and defects. It is based on the principle that irregularities underneath the surface such as holes caused by corrosion or water invasion in a material will affect the thermal energy of that material. These changes in thermal energy will cause different surface temperatures in an object such as a pipe, as seen in **Fig.1.1**. Thus, by observing the surface temperature distribution along the material, the existence and location of any anomaly can be determined (Milovanovic, 2016).

The infrared thermography has proved to be accurate, convenient, and economical for different applications. Nowadays, the method is effectively applied for detection and characterization of cracks and defects in areas, such as the construction and the automotive industry. The use of the infrared thermography method has increased over the last years due to the advance of the infrared cameras, the significant decrease in their cost and the fact that it is a repeatable and a non-destructive testing technique. Which means that there is no contact between the material under investigation and the testing equipment, thus, it is a preferred method due to the reliability of testing (Stanislav, 2012).

Because of the many advantages and promising great developments that the infrared thermography technique has, this approach has been selected to deeply evaluate the defects that exist on the interface between the cement and the casing usually known as micro-annulus.

During cement evaluation downhole, the quality of cement is determined based on the log response. CBL and ultrasonic logs can assess only the state of the internal micro-annulus, but the presence of gaps can exist in both interfaces between the cement casing (the internal and the external). A graphical representation of both cases, the internal and the external is presented in **Fig.1.2**.

Surface crack or defect detection between the casing and the cement is important because it can help to predict leakage channels, therefore, implementing this technique as a micro-annuli size detection has the potential to be of great interest for the operators and logging services companies, especially during the plug and abandonment phase (P&A). Up to now, there is no available technology to evaluate the quality of the external interface bonding (external micro-annulus) and the infrared thermography method can be used as a complementary technique to the logs to characterize the cement quality and leakage potential in the laboratory.

Figure 1.1 *Infrared Thermography technique along a pipe (Menanteau, 2013)*

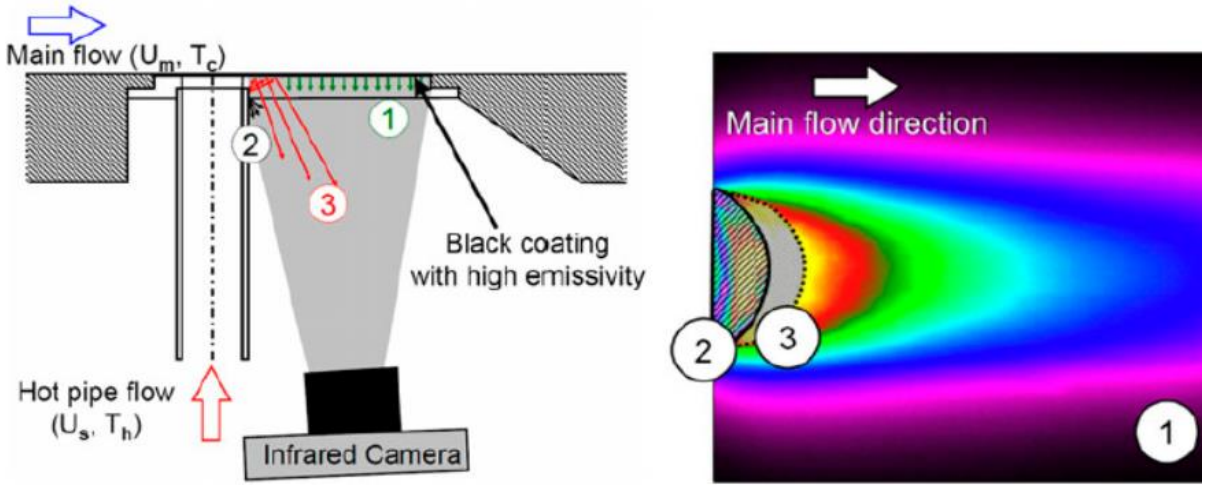

Figure 1.2 *Separation between casing and cement (FMC Technologies, 2013)*

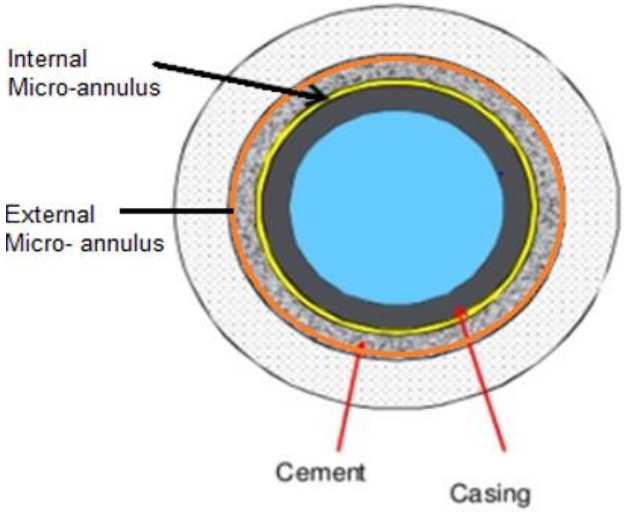

Modified from the source

1.1 Objective

This thesis principally intends to use the infrared thermography technique as a micro-annuli detection tool. The annular cement may have some defects like leakage paths, and this work presents an study of the leakage properties of water through the cemented annulus of a section composed by two casings (7” and 9 5/8”) with cement class G in between. The Darcy-Weisbach equation and the Manning’s equation are used to understand zonal isolation and crossflow of formation fluids.

The migration path geometry and how water and other fluids behave in such paths are evaluated. This study helps to understand how leakage rates can be associated with different micro-annuli sizes or vice versa.

In addition, wall temperature analyses are done by comparing the measured surface temperatures of two sections with the estimated surface temperature values using a proposed indirect measurement technique derived for this study under steady-state conditions. This helps to roughly estimate the surface temperature of a pipe based on the fluid inside, thus, identify a potential flow channel.

2. Methodology

In this study, wall temperature of two different pipes, known as sections C6 and A2 are analyzed. Details can be consulted in **Table 2.1**. Two infrared thermography cameras Seek were used to record thermal images along the sections, in this case they are known as NORCE camera and UiS camera. The camera FOV of 57 degrees and IR chip resolution is 320x240 defines the coverage that can be achieved and associated spatial resolution per pixel.

Table 2.1 *Data of the two sections*

Section	Length (m)	Channel Minnimum Height (mm)	Channel Maximum Height (mm)
C6	8.8	1.5	15
A2	9.7	1	1.5

Hot and cold water were flooding along the cells. The pipes were instrumented with temperature sensors installed in the external surface. Two were installed at the ends (inlet and outlet) and one in the middle, as seen in **Fig.2.1**. Also, pressure sensors were placed at the initial and final part of the cell. To facilitate the images interpretation, a reflective tape was placed every meter to create divisions along the pipe. Both sections are used to study the changes in surface temperature, thus, evaluate the presence of leakage paths. A schematic diagram of the setup is shown in **Fig.2.2**.

Figure 2.1 *Sensors installed for the experiments*

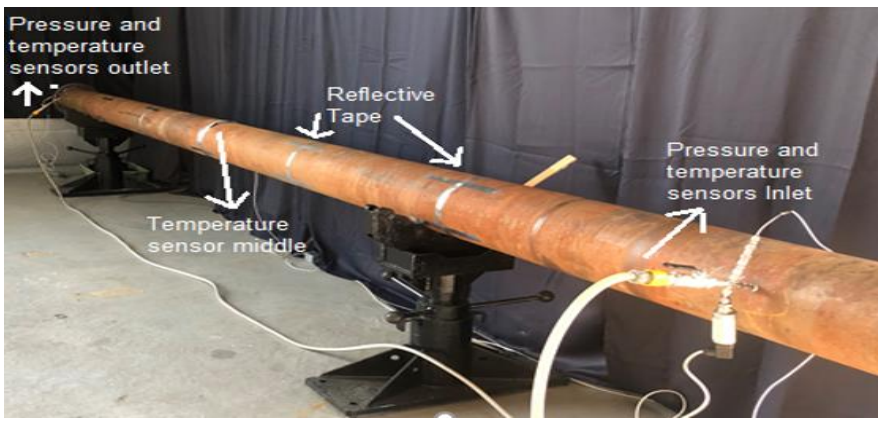

Figure 2.2 *A graphical representation of the experiment setup*

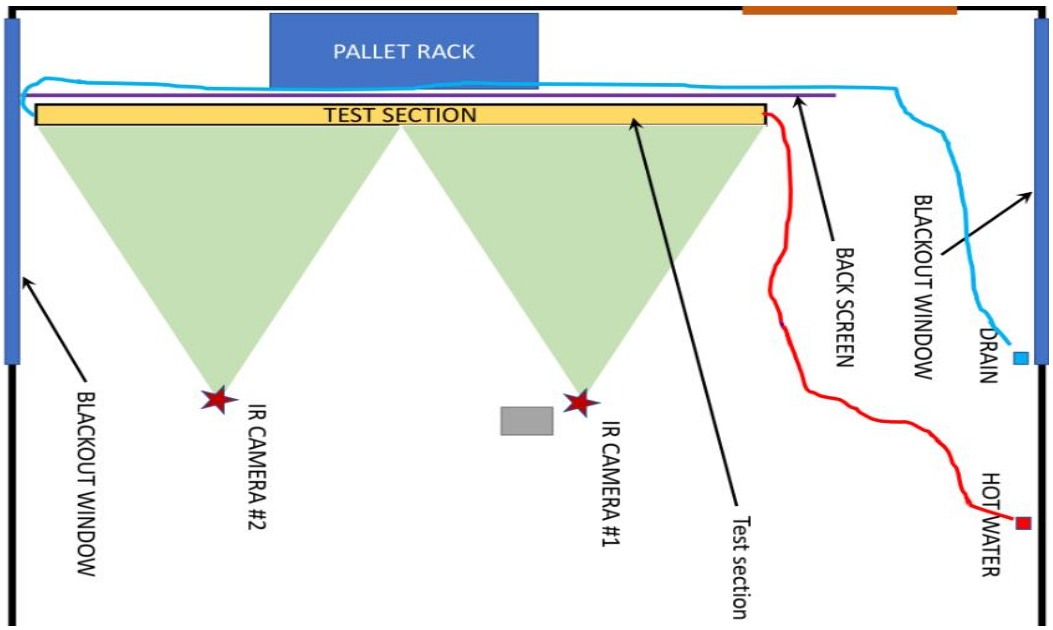

For the section C6, three experiments were performed at different times, each with a different duration. For the section A2, two experiments were performed at different times, each with a different duration. The data recorded by the temperature sensors are shown in **Table 2.2** to **2.5**.

Section C6

To carry out the experiments, important parameters are taken into consideration such as the NORCE-camera temperature range (12- 47°C), UiS-camera temperature range (7- 42°C), cameras-casing horizontal distance (330cm), floor-camera distance (144cm) and height of casing axis (center: 83cm).

Experiment #1: Six meters of pipe are flooding

Table 2.2 *Recorded times with their corresponding data obtained by temperature sensors*

Time	Operation	Tin (°C)	Tsurface middle (°C)	Tout (°C)
10:28	First picture taken	9.96	12.74	11.38
10:30	Start hot water injection	10.03	12.77	11.39
10:50	Stop hot water injection	45.22	38.53	38.04
10:58	Flow rate recorded	32.54	27.10	25.50
11:00	Start cold water injection	31.80	26.04	24.16
11:06	Flow rate recorded	7.81	13.73	13.72
11:12	Stop cold water injection -turning of the pipe	7.73	13.19	11.87
11:15	End of the experiment	9.22	14.87	12.30

Experiment #2: The previous experiment is repeated changing the position of the cameras

Table 2.3 *Recorded times with their corresponding data obtained by temperature sensors*

Time	Operation	Tin (°C)	Tsurface middle (°C)	Tout (°C)
13:00	Start hot water injection	13.62	15.25	10.97
13:03	No change is evident, continue	26.40	15.89	13.00
13:08	Stop due to plugging in the outlet line	24.64	15.58	13.52
13:25	Restart with hot water injection (first picture)	15.55	16.03	15.70
13:26	Flow rate recorded	15.23	15.83	15.38
13:27	Camera UiS shows a bug, pic taken again	27.24	16.38	15.53
13:30	Flow rate recorded	41.21	30.33	29.02
13:41	Stop hot water injection - cooling of the pipe	44.57	39.01	39.11
13:52	Start cold water injection	30.68	25.99	25.12
14:02	Stop cold water injection	6.86	10.75	10.00
14:03	Turning of the pipe	7.16	10.94	10.18

Experiment #3: The position of the cameras is the same as in experiment #2. In this case, injection of hot water doing a close recording of the sections in the middle of the cell for 7 minutes is carried out. Unfortunately, the acquisition system did not record any data.

Section A2

To carry out the experiment, important parameters are taken into consideration such as the NORCE-camera temperature range (12- 47°C), UiS-camera temperature range (7- 42°C), cameras-casing horizontal distance (445cm), floor-camera distance (144cm) and height of casing axis (center: 83cm).

Experiment #1: Eight meters of pipe are flooding

Table 2.4 *Recorded times with their corresponding data obtained by temperature sensors*

Time	Operation	Tin (°C)	Tsurface middle (°C)	Tout (°C)
10:04	First picture taken	8.21	11.50	8.58
10:05	Start hot water injection	8.19	11.49	8.43
10:27	Flow rate recorded	30.05	13.89	11.26
10:34	Flow rate recorded	30.16	14.63	11.75
10:45	Flow rate recorded	30.34	16.45	13.27
10:47	Flow rate recorded	30.51	16.72	13.58
10:50	Flow rate recorded	31.31	17.51	14.19
10:55	Flow rate recorded	31.34	18.33	14.80
11:00	Flow rate recorded	29.91	18.72	15.22
11:05	Flow rate recorded	28.60	18.95	15.44
11:10	Flow rate recorded	29.38	19.30	15.84
11:15	Flow rate recorded	29.56	19.49	16.03

11:20	Stop hot water injection	29.17	19.75	16.22
11:25	Cooling of the pipe (5min)	24.53	18.04	14.61
11:26	Start cold water injection	23.51	17.64	14.23
11:28	Fast increase in leakage rate	12.12	17.64	15.00
11:30	Flow rate recorded	8.43	14.20	13.77
11:36	Closing the hose	7.60	10.99	10.90
11:37	Turning of the pipe	7.71	10.88	10.78

Experiment #2: A second experiment considering only four meters of pipe is performed, the two meters close to the ends are not considered in this case

Table 2.5 *Recorded times with their corresponding data obtained by temperature sensors*

Time	Operation	Tin (°C)	Tsurface middle (°C)	Tout (°C)
12:35	Start hot water injection	30.81	13.61	11.79
12:36	Flow rate recorded	35.91	19.61	16.28
12:50	Stop hot water injection	49.52	38.77	34.73
12:51	Cooling of the pipe	45.89	36.38	31.94
12:58	Start cold water injection	37.15	25.54	23.63
12:59	Flow rate recorded	15.12	27.59	25.18
13:08	Stop cold water injection	7.63	12.40	12.92
13:09	Turning of the pipe	7.46	12.05	12.46

The surface temperature (°C) shown in **Table 2.2** to **2.5** represents the surface temperature of the pipe at its half-length, while the inlet and outlet temperatures (°C) represent the temperature of the fluid injected, in this case water.

The surface temperature (°C) measured by the sensor at the specific times seen in **Table 2.2** to **2.5** is a direct measurement, meaning that any surface temperature estimation using an indirect method should be validated and compared with this key parameter.

For the purposes of this study, it is assumed that the steady state condition is achieved when no representative changes of more than 1 degree Celsius is recorded by a period of time. This criterion was defined for the C6 and A2 sections based on the inlet, surface, and outlet temperature values.

For a comparison, a one-dimensional heat conduction model is derived **(Eq.4)** and proposed to estimate the surface temperature of the pipe at its half-length based on the inlet and outlet temperatures of the fluid inside.

The **Eq.4** for a steady-state regime is used to estimate the surface temperature and compare it with the known direct measurement. If any correlation between these two numbers is found, the surface temperature of a pipe can be roughly estimated based on the inlet and outlet temperatures of the fluid being injected. It should be emphasized that the equation is valid only for steady-state condition and for transient regimes other formulation must be used. A schematic of the 1-D model is shown in **Fig.2.3**.

Figure 2.3 *A schematic of the 1-D proposed model*

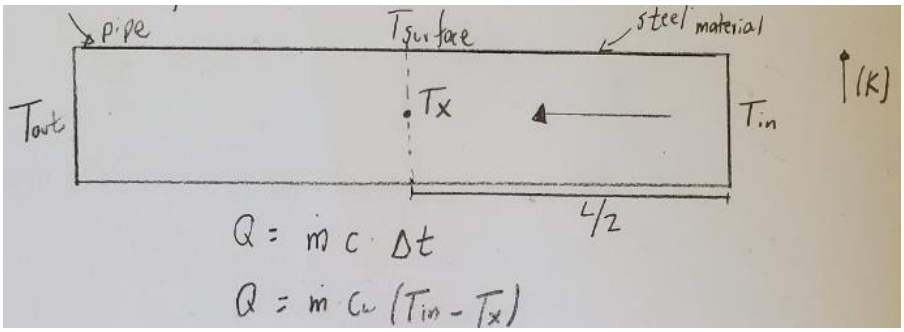

The one-dimensional equation is derived based on two known equations, the quantitative relationship between heat transfer and temperature change **(Eq.1)** and the heat transfer conduction through radial systems in pipes **(Eq.2)** respectively.

$$Q = m * c * \Delta t \quad (1)$$

Where:

- Q = Heat transfer (Watts)
- m = Mass flow rate (kg/s)
- c = Specific heat (Joule/kg - °C)
- Δt = Temperature change (°C)

$$Q = \frac{2 * \pi * k\,(Ti - To) * L}{\ln(\frac{ro}{ri})} \quad (2)$$

Where:

- Q = Heat transfer (Watts)

- k = Thermal conductivity of steel (Watts/ m - °C)
- Tin = Inlet temperature (°C)
- Tout = Outlet temperature (°C)
- L = Length of pipe (m)
- ro = Outer radius (4.8125 in)
- ri = Inner radius (4.2692 in)

In the case of a steady-state heat transfer through a cylindrical pipe, heat is not generated (Eckert, 1959), thus, the general heat conduction is reduced to:

$\frac{d^2T}{dx^2} = 0$ 1. $T(x) = C1(x) + C2$ 2. $T(0) = 0 + C2 => C2 = Tin$

3. $T\ (l) = C1(l) + Tin = Tout$ 4. $C1 = \frac{Tout - Tin}{l}$

Replacing 2 and 4 in 1:

$$T(x) = \left(\frac{Tout - Tin}{l}\right)x + Tin \ => \quad T\left(x = \frac{l}{2}\right) = \left(\frac{Tout - Tin}{l}\right)\left(\frac{l}{2}\right) + Tin$$

$$T\left(x = \frac{l}{2}\right) = \frac{Tout + Tin}{2} \tag{3}$$

Setting **Eq.1** = **Eq.2** and using **Eq.3** for Tx, the surface temperature at half-length is estimated as follows:

$$m\ * cw\ * (Tin - Tx) = \frac{2 * \pi\ * k\ (steel) * (Tx - Tsurface) * (\frac{l}{2})}{\ln(\frac{ro}{ri})}$$

Solving for Tsurface:

$$\frac{m\ * cw\ * (Tin - Tx) * \ln(\frac{ro}{ri})}{2 * \pi\ * \left(\frac{l}{2}\right) * k\ (steel)} = Tx - Tsurface$$

$$Tsurface\ (°C) = Tx - \frac{m\ * cw\ * (Tin - Tx) * \ln(\frac{ro}{ri})}{2 * \pi\ * \left(\frac{l}{2}\right) * k\ (steel)} \tag{4}$$

To calculate the flow rates of different leakage channel center heights, two equations were used, the Darcy-Weisbach and the Manning's equation. A graphical representation of the flow channel can be seen in **Fig.2.4**.

Figure 2.4 *Leakage channel between casing and cement*

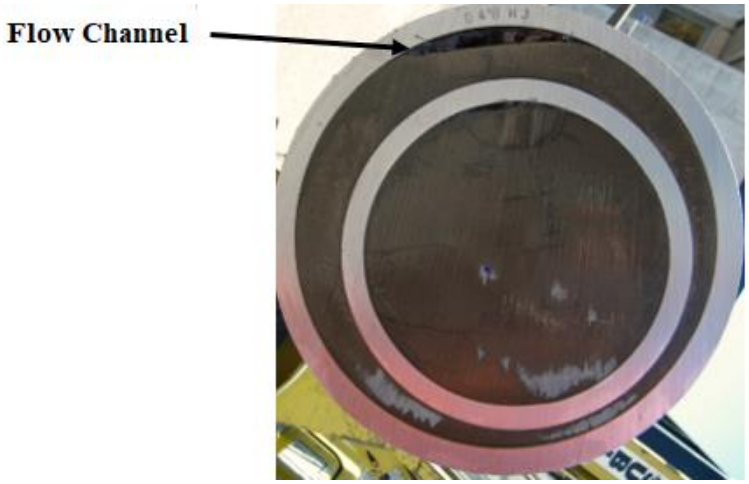

The Darcy-Weisbach equation for volumetric flow rate is an empirical equation developed by integrating other equations. This equation **(Eq.8)** accounts for the pressure loss due to friction, the hydraulic diameter, the length of a given pipe and the dynamic viscosity of a fluid.

The Darcy-Weisbach formula **(Eq.8)** calculates the friction loss in pipes and other conduits when liquids or gases are moved from one point to another, and as a result, for some experiments more accurate flow rate calculations can be estimated (Brown, 2017). For a cylindrical pipe with uniform diameter, **Eq.5** is described as the Darcy-Weisbach equation based on the pressure-loss due to friction**.**

$$\frac{\Delta P}{L} = f_D * \frac{\rho}{2} * \frac{V^2}{D} \tag{5}$$

Where:

- ΔP = Pressure loss (Pa)
- L = Length of pipe (m)

- f_D = Darcy-Weisbach friction factor (dimensionless)
- ρ = Density of the fluid (kg/m^3)
- V = Average flow velocity (m/s)
- D = Hydraulic diameter of pipe (m)

Knowing that the Darcy-Weisbach friction factor, also called resistance coefficient is inversely proportional to the Reynolds number **(Eq.6)** in case of laminar flow, the equation for flow rate calculation can be expressed as **Eq.8**.

$$Re = \frac{\rho * V * D}{\mu} \tag{6}$$

Where:

- Re = Reynolds number (dimensionless)

  Re < 2000 Laminar flow

  2000 < Re < 4000 Transient flow

  Re > 4000 Turbulent flow
- ρ = Density of the fluid (kg/m^3)
- V = Fluid velocity (m/s)
- D = Pipe diameter (m)
- μ= Dynamic viscosity of the fluid (kg/m-s)

Darcy-Weisbach friction factor for laminar flow– Reynolds number relationship:

$$f_D = \frac{64}{Re} \tag{7}$$

Substituting **Eq.6** and **Eq.7** into **Eq.5**:

$$\frac{\Delta P}{L} = \frac{64}{\frac{\rho * V * D}{\mu}} * \frac{\rho}{2} * \frac{V^2}{D}$$

Solving for flow rate (Q):

$$Q(\frac{m^3}{s}) = \frac{\pi * {D_h}^4 * \Delta P}{128 * \mu * L} \quad (8)$$

In case of turbulent flow, the Colebrook-White formula **(Eq.9)** is used to calculate the friction factor (f_D).

$$\frac{1}{\sqrt{f_D}} = -2 \log \left(\frac{k}{3.71 * Dh} + \frac{2.51}{Re * \sqrt{f_D}}\right) \quad (9)$$

Where:

- f_D = Darcy-Weisbach friction factor (dimensionless)
- k = Surface roughness (m)
- Dh = Hydraulic diameter of pipe (m)
- Re = Reynolds number (dimensionless)

Friction losses in pipe flow and open-channel flows are related to the flow type, the fluid properties, and the geometry of the system (Chanson, 2004). To determine if the flow pattern in a system is laminar, transient, or turbulent, a dimensionless number called Reynolds number is used and it can be calculated with **Eq.6**. The Reynolds number relates the inertia forces to the viscous forces, meaning that the effect of the viscosity as a fluid property is an important parameter to be considered (Rehm, 2009).

For the purposes of this study, the Darcy-Weisbach equation is used to estimate the flow rates of different leakage channel heights. However, this equation assumes steady state and incompressible flow with some limitations for turbulent flows (Chanson). Therefore, another formula called the Manning's equation is used in this study to account for turbulent flows, since turbulent flows through pipes are more common than laminar flows.

The Manning's equation is an empirical equation derived based on observation and experience. The reason why this equation is used in this study as opposed to theoretical knowledge based on principles, is turbulence, as there is not enough scientific information about

turbulence to derive an equation and most pipes and channels flow in turbulent conditions (Czachorski, 2018).

The Manning's equation is commonly used for uniform flow in open channels and for flow calculation in partially full conduits such as pipes. The equation is shown as **Eq.10**.

$$Q = \left(\frac{1.49}{n}\right) * A * (R_h)^{\frac{2}{3}} * S^{1/2} \quad (10)$$

Where:

- Q = Volumetric flow rate passing through the channel (ft^3/sec)
- 1.49 = Units conversion factor
- n = Manning roughness coefficient (dimensionless)
- A = Cross-sectional area of flow (ft^2)
- Rh = Hydraulic radius (ft)
- S = Slope of the channel (dimensionless)

For the purposes of this study, the equations used to calculate the parameters needed in the Manning's equation are derived assuming "more than half full" pipe flow (Bengtson). A graphical representation of the assumption and the equations can be seen in **Fig.2.5**.

Figure 2.5 *Partially Full Pipe Flow Parameters - More Than Half Full (Bengtson, #)*

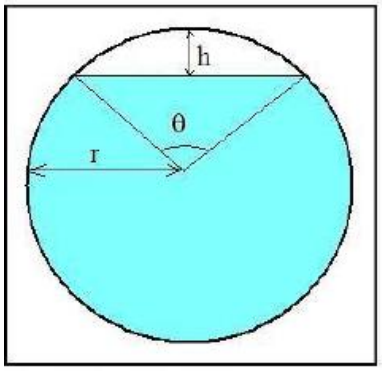

$r = D/2 \qquad h = 2r - y$

$\theta = 2 \arccos\left(\frac{r - h}{r}\right)$

$A = \pi r^2 - \frac{r^2(\theta - \sin\theta)}{2}$

$P = 2\pi r - r\theta$

$R_h = A/P$

However, the case under investigation is not exactly the same as the one seen in **Fig.2.5**, since the flow rate of the empty space above the water with height h (channel) is to be determined in this case, rather than the flow rate of the filled space (blue area). Therefore, the

equations for the cross-sectional area (A) and the wetted perimeter (P) have been modified to estimate only the flow rate of the channel. The new modified equations are **Eq. 11** and **Eq.12**.

$$A = \frac{r^2 * (\theta - sin\theta)}{2} \tag{11}$$

$$P = r * \theta + 2 * r * sin\theta \tag{12}$$

The hydraulic radius (Rh) is the variable that considers the channel shape, in this case the geometry of a pipe at certain level of fill. This parameter is calculated knowing the channel heights of 1mm and 1.5mm for the section A2 and 1.5mm and 15mm for the section C6, respectively. The Rh is the ratio of the cross-sectional area of the flow divided by the wetted perimeter (P), but in the case of an open channel flow, this ratio should be multiplied by 4.

The n value is an empirical constant that changes depending on the roughness of the pipe or channel. This value accounts for the channel friction that is applied to the flow, meaning that if the "n" value is higher, the roughness or toughness of the material is increased (Edwards, 1998).

The S value in a uniform flow is described as the bottom slope of the channel (So), meaning that the slope of the liquid surface (Sw) and the energy line should all be the same (parallel to each other) for a constant depth flow (Finnermore, 2001). A graphical representation can be seen in **Fig.2.6**. For a non-uniform flow, the case is different, and a variation in the slope should be considered.

Figure 2.6 *Slope in open channel flow (Finnermore, 2001)*

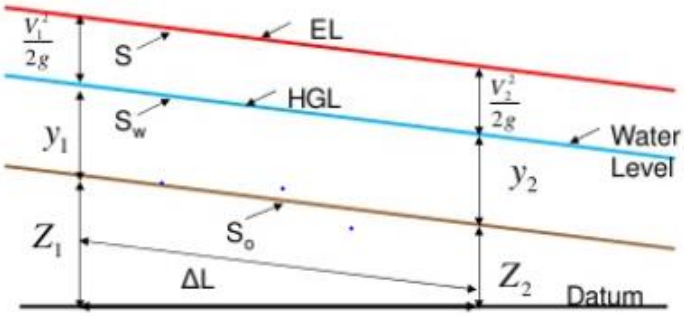

S represents the relation between the energy lost as a function of distance. In the Manning's equation, uniform open channel flow is assumed, meaning that a constant flow rate through a channel with constant friction slope S, roughness and size should exist (Chow, 1959).

In this study, it is known that the height of the channel "h" (empty space above the fluid as seen in **Fig.2.5**) is not the same for the sections A2 and C6, therefore, a variation in the friction slope S and the manning roughness coefficient n must be considered in order to reproduce the experimental conditions.

For the purposes of this study, the friction slope S is assumed to be 0.0001 for case #1, that is assuming there is no variation in the n value for a cast-iron channel surface. For case #2, the friction slope S is assumed to be 1, that is assuming a variation in the n value for a corrugated metal channel surface. The selected open channel materials with their corresponding Manning roughness coefficient "n" can be seen in **Table 2.6**.

Table 2.6 *Typical Manning Roughness Coefficient Values (Chow, 1959)*

Channel Surface	**Manning roughness coefficient (n)**
Cast-iron	0.012
Corrugated metal	0.022

The n value of 0.012 for a cast-iron channel surface is used because it is almost the same as the n value of 0.011 for a steel channel surface, as it is one of the most common materials for pipes and channels. To consider a possible variation in roughness along the cells, additional estimations were calculated using an n value of 0.022 for a corrugated metal channel.

3. Results and Discussion

In order to examine the wall temperature of sections C6 and A2 with more accuracy, the data recorded by the temperature sensors in the experiments shown in **Table 2.2** to **2.5** have been averaged considering a 40-second window. This means that 20 seconds before and 20 seconds after the selected times of the experiments have been considered as the final measured data. The values for section C6 and A2 are shown in **Table 3.1** to **3.2** and **Table 3.3** to **3.4**, respectively.

Section C6

Experiment #1: It has a duration of 47 minutes

Table 3.1 *Averaged data obtained by the temperature sensors*

Time	Operation	Tin (°C)	Tsurface middle (°C)	Tout (°C)
10:28	First picture taken	9.98	12.78	11.39
10:30	Start hot water injection	10.29	12.79	11.50
10:50	Stop hot water injection	45.18	38.52	37.85
10:58	Flow rate recorded	32.56	27.10	25.50
11:00	Start cold water injection	32.70	26.12	24.86
11:06	Flow rate recorded	7.83	13.74	13.77
11:12	Stop cold water injection -turning of the pipe	7.69	13.17	11.84
11:15	End of the experiment	9.25	14.89	12.33

Experiment #2: It has a duration of 63 minutes

Table 3.2 *Averaged data obtained by the temperature sensors*

Time	Operation	Tin (°C)	Tsurface middle (°C)	Tout (°C)
13:00	Start hot water injection	18.59	15.25	11.32
13:03	No change is evident, continue	26.49	15.87	12.98
13:08	Stop due to plugging in the outlet line	24.77	15.58	13.53
13:25	Restart with hot water injection (first picture)	15.53	16.01	15.68
13:26	Flow rate recorded	14.54	15.85	15.38
13:27	Camera UiS shows a bug, pic taken again	27.14	16.60	15.78
13:30	Flow rate recorded	41.16	30.33	28.97
13:41	Stop hot water injection - cooling of the pipe	44.57	39.02	39.08
13:52	Start cold water injection	30.05	26.15	26.40
14:02	Stop cold water injection	6.88	10.77	10.01
14:03	Turning of the pipe	7.16	10.97	10.14

Section A2

Experiment #1: It has a duration of 93 minutes

Table 3.3 *Averaged data obtained by the temperature sensors*

Time	Operation	Tin (°C)	Tsurface middle (°C)	Tout (°C)
10:04	First picture taken	8.20	11.47	8.58
10:05	Start hot water injection	9.17	11.48	8.48
10:27	Flow rate recorded	30.02	13.88	11.24
10:34	Flow rate recorded	30.22	14.63	11.81
10:45	Flow rate recorded	30.33	16.45	13.27
10:47	Flow rate recorded	30.50	16.74	13.59
10:50	Flow rate recorded	31.28	17.51	14.20
10:55	Flow rate recorded	31.37	18.32	14.83
11:00	Flow rate recorded	29.92	18.74	15.21
11:05	Flow rate recorded	28.58	18.94	15.45
11:10	Flow rate recorded	29.37	19.31	15.85
11:15	Flow rate recorded	29.57	19.50	16.05
11:20	Stop hot water injection	29.15	19.75	16.23
11:25	Cooling of the pipe (5min)	24.52	18.03	14.61
11:26	Start cold water injection	23.54	17.64	14.26
11:28	Fast increase in leakage rate	12.08	17.63	15.00
11:30	Flow rate recorded	8.43	14.18	13.76
11:36	Closing the hose	7.62	11.00	10.91
11:37	Turning of the pipe	7.74	10.96	10.79

Experiment #2: It has a duration of 34 minutes

Table 3.4 *Averaged data obtained by the temperature sensors*

Time	Operation	Tin (°C)	Tsurface middle (°C)	Tout (°C)
12:35	Start hot water injection	25.44	13.89	11.76
12:36	Flow rate recorded	35.92	19.56	16.28
12:50	Stop hot water injection	49.46	38.80	34.57
12:51	Cooling of the pipe	45.85	36.36	31.94
12:58	Start cold water injection	35.58	25.77	24.20
12:59	Flow rate recorded	15.61	27.27	25.03
13:08	Stop cold water injection	7.61	12.39	12.89
13:09	Turning of the pipe	7.46	12.05	12.47

In this study, the steady state temperature condition is defined using the three temperature values from **Table 3.1** to **3.3**. The times selected for the steady-state condition can be seen in **Table 3.5**. and **Table 3.6** for section C6 and A2, respectively.

Table 3.5 *Times selected for the analysis of the surface temperature in section C6*

Exp #	Time	Operation	Flow rate(mL/10sec)	Tin (°C)	Tsurface Middle (°C)	Tout (°C)	State
1	10:30	Start hot water injection	680	10.29	12.79	11.50	Not steady
1	10:58	Flow rate recorded	680	32.56	27.10	25.50	Not steady
1	11:06	Flow rate recorded	750	7.83	13.74	13.77	Not steady
2	13:00	Start hot water injection	800	18.59	15.25	11.32	Steady
2	13:03	No change is evident, continue	820	26.49	15.87	12.98	Steady
2	13:08	Stop due to plugging in the outlet line	850	24.77	15.58	13.53	Steady
2	13:25	Restart with hot water injection (first picture)	910	15.53	16.01	15.68	Steady
2	13:26	Flow rate recorded	930	14.54	15.85	15.38	Steady
2	13:27	Camera UiS shows a bug, pic taken again	950	27.14	16.60	15.78	Steady
2	13:30	Flow rate recorded	1000	41.16	30.33	28.97	Not steady

Table 3.6 *Times selected for the analysis of the surface temperature in section A2*

Exp #	Time	Operation	Flow rate(mL/30sec)	Tin (°C)	Tsurface Middle (°C)	Tout (°C)	State
1	10:05	Start hot water injection	230	9.17	11.48	8.48	Not steady
1	10:27	Flow rate recorded	240	30.02	13.88	11.24	Not steady
1	10:34	Flow rate recorded	240	30.22	14.63	11.81	Not steady
1	10:45	Flow rate recorded	350	30.33	16.45	13.27	Not steady
1	10:47	Flow rate recorded	430	30.50	16.74	13.59	Not steady
1	10:50	Flow rate recorded	420	31.28	17.51	14.20	Not steady
1	10:55	Flow rate recorded	400	31.37	18.32	14.83	Steady
1	11:00	Flow rate recorded	410	29.92	18.74	15.21	Steady
1	11:05	Flow rate recorded	430	28.58	18.94	15.45	Steady
1	11:10	Flow rate recorded	460	29.37	19.31	15.85	Steady
1	11:15	Flow rate recorded	480	29.57	19.50	16.05	Steady
1	11:20	Stop hot water injection	470	29.15	19.75	16.23	Steady
1	11:30	Flow rate recorded	2010	8.43	14.18	13.76	Not steady

Then, the surface middle temperature (°C) of **Tables 3.5**. and **3.6** is a direct measurement that is used as a reference point to validate the surface temperature estimated using the one-dimensional heat conduction equation **(Eq.4)**. The estimated surface temperatures using **Eq. 4** are presented in **Table 3.7** and **3.8** for section C6 and A2, respectively.

Table 3.7 *Comparison of the Tsurface measured vs the Tsurface estimated for section C6*

Time	Tin (C°)	Tout (C°)	Tx=(L/2)	Tsurface middle (C°)	Tsurface estimated (C°)	State
10:30	10.29	11.50	10.90	12.79	10.92	Not Steady
10:58	32.56	25.50	29.03	27.10	28.89	Not Steady
11:06	7.83	13.77	10.80	13.74	10.93	Not Steady
13:00	18.59	11.32	14.96	**15.25**	**14.79**	Steady
13:03	26.49	12.98	19.74	**15.87**	**19.42**	Steady
13:08	24.77	13.53	19.15	**15.58**	**18.87**	Steady
13:25	15.53	15.68	15.60	**16.01**	**15.61**	Steady
13:26	14.54	15.38	14.96	**15.85**	**14.98**	Steady
13:27	27.14	15.78	21.46	**16.60**	**21.15**	Steady
13:30	41.16	28.97	35.07	30.33	34.71	Not Steady

Table 3.8 *Comparison of the Tsurface measured vs the Tsurface estimated for section A2*

Time	Tin (C°)	Tout (C°)	Tx=(L/2)	Tsurface middle (C°)	Tsurface estimated (C°)	State
10:05	9.17	8.48	8.83	11.48	8.82	Not Steady
10:27	30.02	11.24	20.63	13.88	20.59	Not Steady
10:34	30.22	11.81	21.02	14.63	20.97	Not Steady
10:45	30.33	13.27	21.80	16.45	21.74	Not Steady
10:47	30.50	13.59	22.05	16.74	21.98	Not Steady
10:50	31.28	14.20	22.74	17.51	22.67	Not Steady
10:55	31.37	14.83	23.10	**18.32**	**23.03**	Steady
11:00	29.92	15.21	22.57	**18.74**	**22.51**	Steady
11:05	28.58	15.45	22.01	**18.94**	**21.96**	Steady
11:10	29.37	15.85	22.61	**19.31**	**22.55**	Steady
11:15	29.57	16.05	22.81	**19.50**	**22.75**	Steady
11:20	29.15	16.23	22.69	**19.75**	**22.63**	Steady
11:30	8.43	13.76	11.10	14.18	11.20	Not Steady

"Tx" in **Table 3.7** and **3.8** is the average of the inlet and outlet temperature of the fluid using **Eq.3**, and **Eq.4** to estimate the pipe surface temperature**.** The flow rates represented by the red color in **Table 3.5** were not recorded, so they are assumed based on a linear drop in the temperature from inlet to outlet.

Comparing the calculated and measured temperature in the middle of the pipe (Tsurface) from **Tables 3.7** and **3.8**, it appears that the numbers are closer during steady-state condition. During the period when the steady-state condition cannot be achieved, the predictions in temperature tend to differ more, which makes sense because **Eq.4** is derived of equations that consider only steady-state condition.

Because the estimated temperatures are relatively similar to the measured values for the two sections, as the best estimation of Tsurface differs 0.4°C and the worst 4.5°C for section C6 and for section A2 the best estimation differs 2°C and the worst 4.7°C from the measured values, thus, it can be said that a correlation exists between the direct measurement and the indirect measurement proposed for this study. Therefore, the surface temperature of a pipe at its half-length can be roughly estimated based on the inlet and outlet temperatures of the fluid being injected.

In addition to estimating the surface temperature of sections C6 and A2 using **Eq.4**, the pictures taken by the two infrared thermography cameras show the temperature profile of the two sections when water is being injected. By doing this, the presence of a channel is detected and an evaluation for leakage path is made. The results for section C6 and A2 are presented in **Fig.3.1** to **Fig.3.4** and **Fig.3.5** to **Fig.3.8**, respectively.

Section C6

Looking at **Fig.3.1** obtained during the first experiment, a change in temperature is visible as the hot water goes from right to left. The channel appears to be uniform for the first three sections identified by the reflective tape. However, a non-uniformity in the leakage path is identified in the cell due to the change of shape in the thermal spectrum.

Figure 3.1 *Observation of a possible non-uniform flow channel*

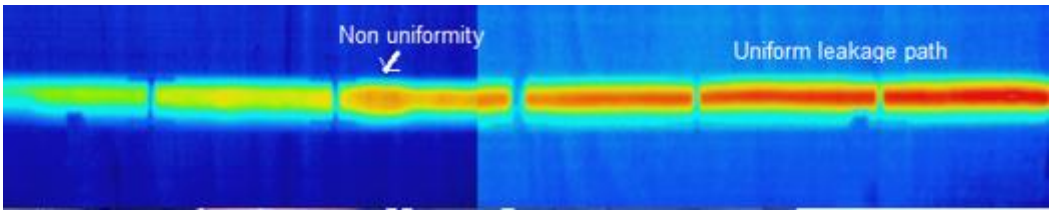

For the second experiment, the cameras switched positions. The picture shown in **Fig.3.2** was taken when the pipe is in the cooling process. At this stage, the temperature decreases on the casing wall and the thermal spectrum contains less red color, confirming that the water inside the leakage pipe is also cooling.

The **Fig.3.3** shows the thermal profile when the pipe is flooded with cold water, and the thermal spectrum shows that the casing wall is cooler in the leakage path location, showing a darker blue color. The same non-uniformity in the flow channel is identified in this experiment. Thus, the observations during the first experiment are confirmed.

Figure 3.2 *Verification of non-uniform flow channel while cooling the pipe*

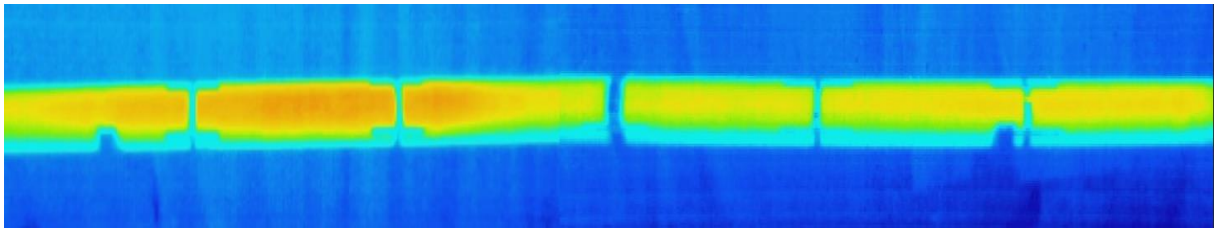

Figure 3.3 *Verification of non-uniform flow channel with cold water*

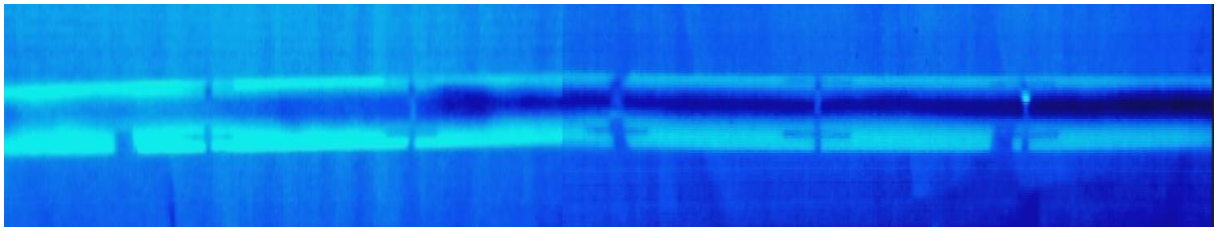

Lastly, in the third experiment, hot water is injected again and after rotating the pipe to check for changes in temperature, a close-up view **(Fig.3.4)** confirms the heating only in the main channel. Therefore, from **Fig.3.1** to **Fig.3.4** it is proven that the channel is not completely uniform.

Figure 3.4 *A close-up view of the rotation*

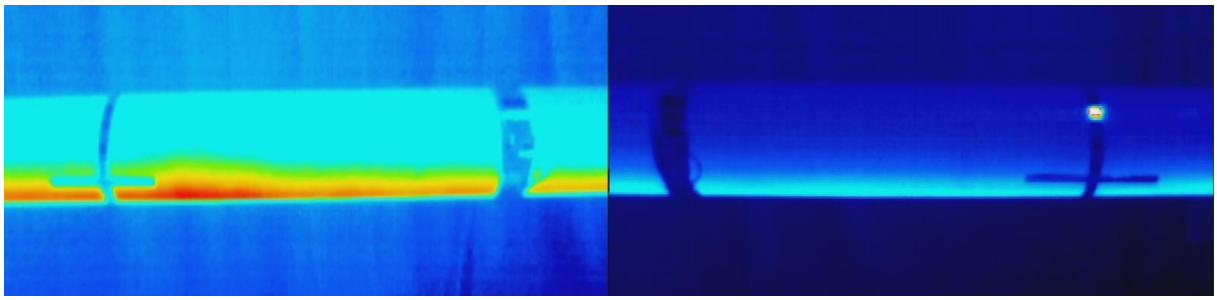

It should be emphasized that the bright spot seen in the right side of **Fig.3.4** is just an artefact due to a reflection of the light in the reflective tape and it does not mean that there is change of temperature in that area. For the purposes of these experiments, the NORCE-camera

had a fixed temperature range of 12-47°C, while the UiS-camera had a fixed temperature range of 7– 42°C, which that explains the different tonality in the pictures.

Section A2

Looking at **Fig.3.5** obtained during the first experiment, the same change in temperature is visible as the hot water goes from inlet to outlet (right to left). For this section, the channel is more uniform throughout the pipe, with less changes in shape and well-defined contours.

Figure 3.5 *Observation of a possible uniform flow channel*

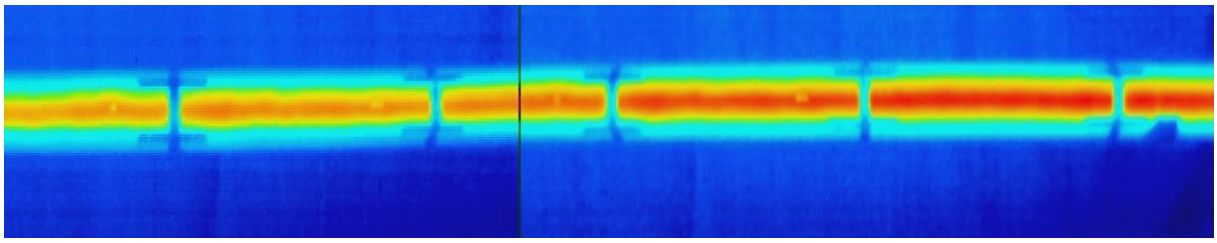

For the second experiment, **Fig.3.6** shows the pipe in the cooling process. **Fig.3.7** shows the pipe flooded with cold water, and not a visible anomaly or irregularity can be seen. Thus, observations during the first experiment are confirmed.

Figure 3.6 *Verification of uniform flow channel while cooling the pipe*

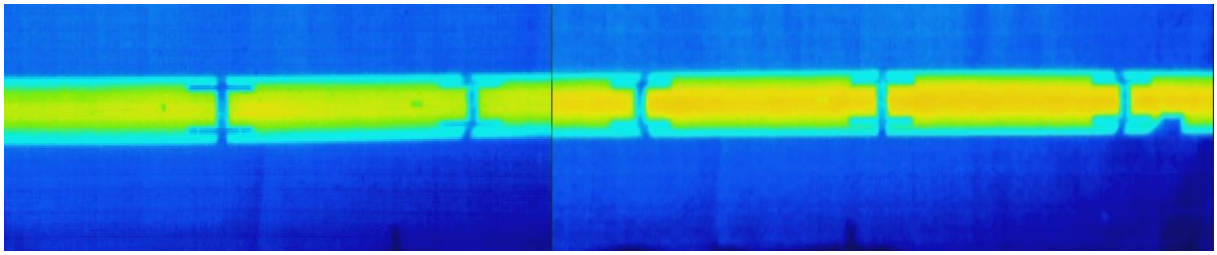

Figure 3.7 *Verification of uniform flow channel with cold water*

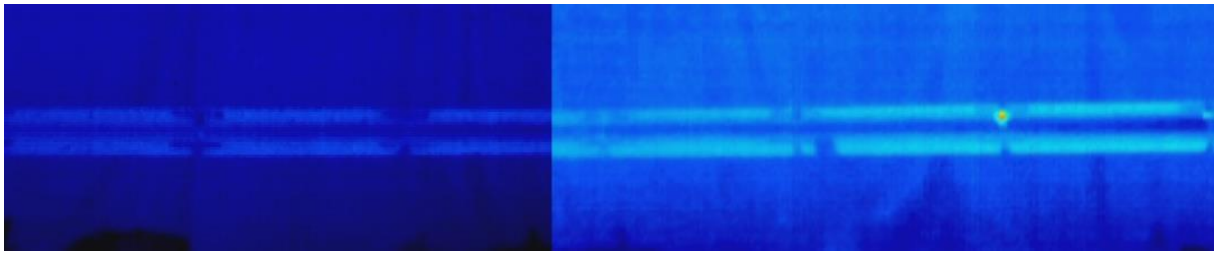

Lastly, when the pipe is fully filled with cold water, it is rotated to check for temperature changes **(Fig.3.8)**, and as a result, the presence of one main channel along the pipe is confirmed.

Therefore, from **Fig.3.5** to **3.8,** it is proven that the channel is uniform throughout the section and that the micro-annulus is homogeneous.

Figure 3.8 *A rotational view of the section filled with cold water*

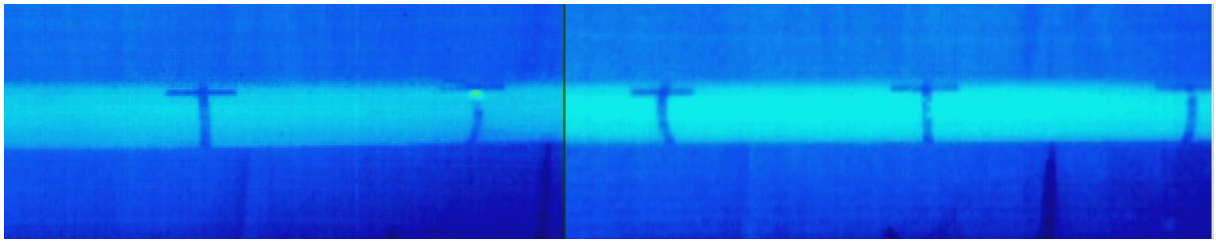

It should be emphasized that the bright spot seen in the right side of **Fig. 3.7** and the left side of **Fig 3.8** is just an artefact due to a reflection of the light on the reflective tape and it does not mean that there is heat in those areas. Also, it is important to know that the two meters close to the ends of the pipe are not considered in the second experiment.

For the purposes of these experiments, the same calibration problem in the temperature range of the two cameras is the explanation of the different tonality in the pictures.

For the second part of the thesis study, flow rates of different known channel heights in sections C6 and A2 are estimated using two equations, the Darcy equation, and the Manning's equation.

In the Darcy equation **(Eq.8)**, it is assumed that the channel has a circular cross-sectional area and the pressure has no dependency with the viscosity. A water viscosity of 0.000797 Pa-s at 30°C is assumed. The hydraulic diameter in this case is $Dh = 4 * \frac{A}{P}$, where A is obtained with **Eq.11** and P with **Eq.12**, respectively. Also, the inlet and outlet pressures used in the calculations were recorded by sensors, which can be seen in the Appendix. The estimations of flow rate using the Darcy equation are presented in **Table 3.9** and **Table 3.10** for section C6 and A2, respectively.

Table 3.9 *Estimation of the flow channel rate in section C6*

Channel Height (mm)	Θ (radians)	Area (m^2)	Wetted P (m)	Dh (m)	Flow Rate (l/min)
1.5	0.33310	0.00004	0.10700	0.00135	0.65608
15	1.06467	0.00112	0.30503	0.01464	9199.80911

Table 3.10 *Estimation of the flow channel rate in section A2*

Channel Height (mm)	Θ (radians)	Area (m^2)	Wetted P (m)	Dh (m)	Flow Rate (l/min)
1	0.27187	0.00002	0.08769	0.00089	0.09368
1.5	0.33310	0.00004	0.10700	0.00135	0.48006

Comparing the estimated flow rates from **Tables 3.9** and **3.10** with the measured values seen in **Table 3.11**, the numbers differ. For section C6, the measured leakage rate is between 4.08 and 6 liters/min, which is equivalent to an effective channel size of 2.5mm. For section A2, the measured leakage rate is between 0.47 and 0.88 liters/min, which is equivalent to an effective channel size between 1.5mm and 2mm. These estimations can be seen in the Appendix.

The variation in the estimated flow rates presented in **Tables 3.9** and **3.10** could be due to the assumptions made in the Darcy formula along with its limitations for turbulent flows. Regarding the measured flow rates seen in **Table 3.11**, they are just the average of the measured flow rates seen in **Tables 3.5** and **3.6** for section C6 and A2, respectively.

Table 3.11 *Measured flow channel rates for section C6 and A2*

Section	Measured Flow Rate Min (l/min)	Measured Flow Rate Max (l/min)
C6	4.08	6
A2	0.47	0.88

In the Manning's equation **(Eq.10)**, the assumption of "more than half full" pipe flow **(Fig.2.5)** is made and the modification in the cross-sectional area and the wetted perimeter is considered to estimate only the hydraulic radius of the flow channels. Also, the "n" value for a

cast-iron channel surface is initially used for the flow rate estimations (case #1), but since it is known that the channel height varies from one section to another, a variation in the "n" value is considered assuming a corrugated metal channel surface (case #2) to investigate the effect of roughness in the flow rate estimations. Finally, the S value is assumed based on the uniformity of the channel, as it represents the energy lost as a function of distance. The results using the Manning's equation are presented in **Table 3.12** and **Table 3.13** for section C6 and A2, respectively.

Table 3.12 *Estimation of the flow channel rates in section C6*

Channel Height (mm)	Θ (radians)	Area (ft^2)	Wetted P (ft)	Rh (ft)	n (case #1)	Q case #1 (l/min)	n (case #2)	Q case #2 (l/min)
1.5	0.33258	0.00039	0.35161	0.00441	0.01023	0.02584	0.02251	1.17443
15	1.06296	0.01204	1.00271	0.04802	0.01167	3.44975	0.02568	156.80694

Table 3.13 *Estimation of the flow channel rates in section A2*

Channel Height (mm)	Θ (radians)	Area (ft^2)	Wetted P (ft)	Rh (ft)	n (case #1)	Q case #1 (l/min)	n (case #2)	Q case #2 (l/min)
1	0.27144	0.00021	0.28816	0.00293	0.01015	0.01080	0.02234	0.49090
1.5	0.33258	0.00039	0.35161	0.00441	0.01023	0.02584	0.02251	1.17443

Comparing the estimated flow rates from **Tables 3.12** and **3.13** with the measured values seen in **Table 3.11**, the numbers differ for the two cases in section C6, however, in section A2 the numbers seem to be close to the measured values for case #2, this can be explained because section A2 has a uniform channel and the friction losses in this case have less influence, unlike section C6 where the channel is not uniform.

It is also important to know that using the variation in the "n" value (case #2) is expected to reproduce better the real conditions, as it accounts for the height change and friction losses. A comparison of all the estimated flow rates can be seen in **Table 3.14** and **3.15** for section C6 and A2, respectively.

Table 3.14 *Comparison of the measured flow rates vs the estimated flow rates in section C6*

Channel Height (mm)	Measured (l/min)	Manning's with variation (l/min)	Manning's no variation (l/min)	Darcy @30°C (l/min)
1.5	4.08	1.1	0.03	0.66
15	6	156	3.5	9199

Table 3.15 *Comparison of the measured flow rates vs the estimated flow rates in section A2*

Channel Height (mm)	Measured (l/min)	Manning's with variation (l/min)	Manning's no variation (l/min)	Darcy @30°C (l/min)
1	0.47	0.49	0.01	0.09
1.5	0.88	1.1	0.03	0.48

4. Conclusions

Leakage properties were studied using two sections composed by two casings and conventional cement class G in the annular space. Leakage measurements and IR thermography were used to assess the relationship between leakage rate and channel size using a total of 113 pictures for section C6 and 128 pictures for section A2. The application of the IR thermography proved to be a useful tool to detect the location of cement defects, such as leakage paths.

Using the two infrared thermography cameras, it was possible to identify changes in thermal profiles and non-uniformities, as for example the non-uniformity found in section C6. For section A2, experiments and pictures revealed that the channel is more uniform and homogenous throughout the pipe in comparison with section C6.

The one-dimensional heat conduction model used to estimate the surface temperature of a pipe presented better results when the steady-state condition is achieved. In conditions where steady state cannot be reached, this equation is not applicable. However, representative differences between the estimated and measured temperatures were found, even in steady-state condition. Suggesting a potential for future research considering transient analysis for example to evaluate improvements in prediction of surface casing temperature.

Regarding the estimations of the flow rates using the Darcy equation, important differences were found when compared estimations to the measured values. This could be due to the model limitations as for example those regarding with turbulent flow, as turbulence is more common in pipes and channels and in this case is not considered.

Regarding the estimations of the flow rates using the Manning's equation, it can be concluded that according to the experiments in section C6 for case #1 and case #2, differences are more representative when estimated flow rates are compared to the measured ones. For section A2, the numbers for case #2 are closer to the measured values. This can be associated with the evidence of a more uniform channel found in the section A2, which can have some effects in the energy losses inside the leakage path. However, this equation should be used carefully once that the estimations are very sensitive to variations in the Manning's roughness coefficient (n). Once that these coefficients are not constant, but depend primarily on the relative roughness (and therefore the absolute roughness characterizing the state of the wall of the channel), the aspect ratio of the area on the Reynolds number demonstrates the effect of kinematic viscosity.

5. References

1. Bengtson, H.H. *Spreadsheet Use for Partially Full Pipe Flow Calculations* [Lecture notes]. Continuing Education and Development. Accessed 10 April 2020. https://www.cedengineering.com/userfiles/Spreadsheet%20Use%20for%20Partially%20Full%20Pipe%20Flow%20Calculations.pdf
2. Cameron, I. (2013, April 16). *SPE "Back to Basics" Bond Log Theory and Interpretation* [PowerPoint slides]. SlideShare. https://www.slideshare.net/AbdelghaniBrikat/bond-log-theory-and-interpretation
3. Camp, T. (1946). Design of Sewers to Facilitate Flow. *Sewage Works Journal*, 18 (3)
4. Cengel, Y.A. (2002). *Heat Conduction Equation.* 2nd Edition. McGraw-Hill Book Company.
5. Chanson, H. (2004). *Environmental Hydraulics for Open Channel Flows*. Butterworth-Heinemann. https://www.sciencedirect.com/book/9780750661652/environmental-hydraulics-of-open-channel-flows
6. Chaudhry, A.U. (2004). *Oil Well Testing Handbook*. Gulf Professional Publishing. https://www.sciencedirect.com/book/9780750677066/oil-well-testing-handbook
7. Chow, V. (1959). *Open- Channel Hydraulics*. New York, McGraw-Hill Book Company
8. Czachorski, R. (2018, March 28). *Manning's Equation-The Details Behind this Highly Versatile Formula.* H2Ometrics. https://www.h2ometrics.com/manning-equation/
9. Darcy-Weisbach equation. (2020, May 21). In *Wikipedia*. https://en.wikipedia.org/wiki/Darcy%E2%80%93Weisbach_equation#:~:text=In%20fluid%20dynamics%2C%20the%20Darcy,flow%20for%20an%20incompressible%20fluid.
10. Eckert, E.R.G. & Drake, R.M. (1959). *Heat and Mass Transfer*. McGraw-Hill Book Company

11. Edwards, K. (1998). *Manning Equation - Fluid Flow Calculations*. LMNO Engineering. https://www.lmnoeng.com/manning.php

12. Finnermore, E. & Franzini, J. (2001). *Fluid Mechanics with Engineering Applications*. 10th edition. McGraw-Hill Education

13. Hassan, M. (2015). *Applied Thermodynamics and Heat Engines* [PowerPoint slides]. SlideShare.

    https://www.slideshare.net/vjtiprod/thermodynamics-chapter-3-heat-transfer

14. *Manning's Equation.* (2006). FishXing- Hydraulic Reference. http://www.fsl.orst.edu/geowater/FX3/help/1_TOC/Hydraulic_Reference_TOC.htm

15. Menanteau, S., Bougeard, D., Harion, J.L. & Muller, T. (2013). Wall temperature fluctuations measurements downstream of a pipe junction using infrared thermography. *Quantitative Infrared Thermography, Vol.10*, No.2, 172-187, http://dx.doi.org/10.1080/17686733.2013.800691

16. Mendez, M., Teodoriu, C., Salehi, S., & Wu, X. (2020). A novel way to look at the cement sheath integrity by introducing the existence of empty spaces inside of the cement (voids). *Journal of Natural Gas Science and Engineering.*

    https://doi.org/10.1016/j.jngse.2020.103274

17. Menon, E.S. (2015). Fluid Flow in Pipes. *ScienceDirect.*

    https://www.sciencedirect.com/topics/engineering/reynolds-number

18. Milovanovic, B., Pecur, I.B. (2016). Review of Active IR Thermography for Detection and Characterization of Defects in Reinforced Concrete. *Journal of Imaging.*

    https://www.researchgate.net/publication/299842596_Review_of_Active_IR_Thermography_for_Detection_and_Characterization_of_Defects_in_Reinforced_Concrete

19. *Normal Flow Equations and Friction Head Loss*. Basic Concepts Related to Flowing Water and Measurement. Accessed 15 May 2020.

    https://www.usbr.gov/tsc/techreferences/mands/wmm/chap02_16.html

20. Normani, F. (2004). *Heat Exchanger*. Real World Physics Problems.

https://www.real-world-physics-problems.com/heat-exchanger.html

21. Rehm, B., Schubert, J., Haghshenas, A., Paknejad, A.S & Hughes, J. (2009). *Managed Pressure Drilling*. Gulf Publishing Company.

https://www.sciencedirect.com/book/9781933762241/managed-pressure-drilling

22. Runnemalm, A., Broberg, P. (2014). *Surface Crack Detection Using Infrared Thermography and Ultraviolet Excitation*. University West.

https://www.ndt.net/article/qirt2014/papers/QIRT-2014-016.pdf

23. Stanislav, S., Matz, V. (2012, June 18-21). *Automated System for Crack Detection Using Infrared Thermographic Testing*. 4th International CANDU In-service Inspection Workshop and NDT Conference, Canada.

https://pdfs.semanticscholar.org/e7a6/054018cfd8479c4ed4ab1a699204e0950b90.pdf

24. Steel, E.W. & McGhee, T.J. (1979). *Water Supply and Sewerage*, 5th Ed., New York, McGraw-Hill Book Company.

Appendix

Data registered by the pressure and temperature sensors for Section C6

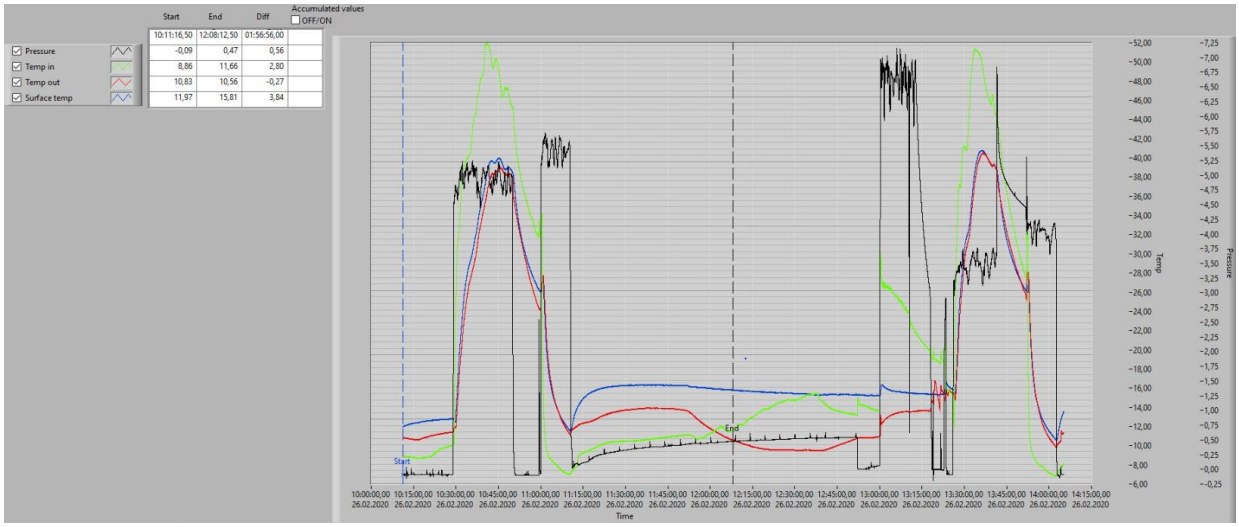

Data registered by the pressure and temperature sensors for Section A2

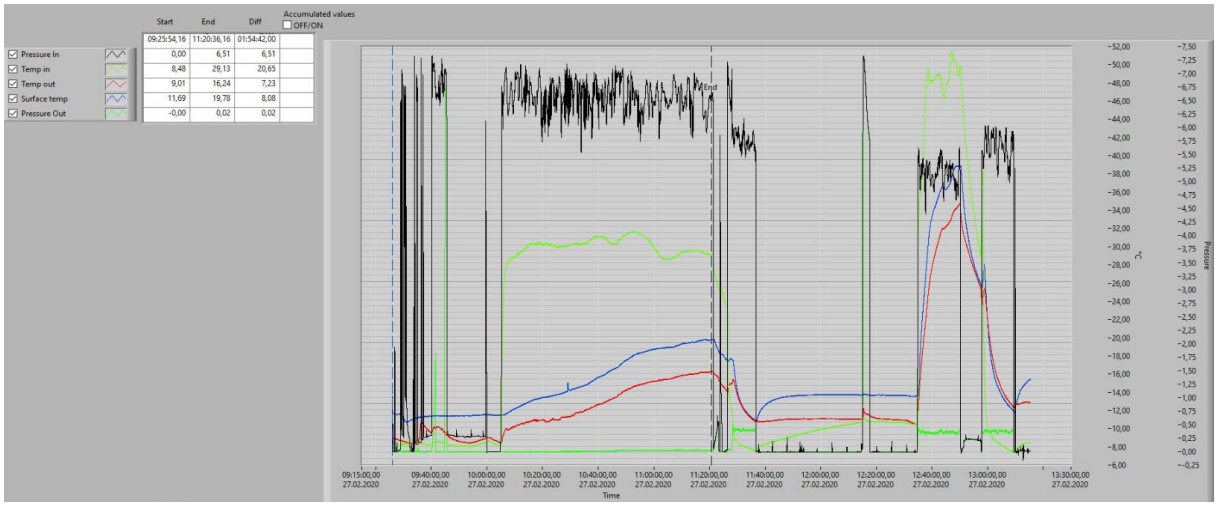

Time versus Temperature for section C6

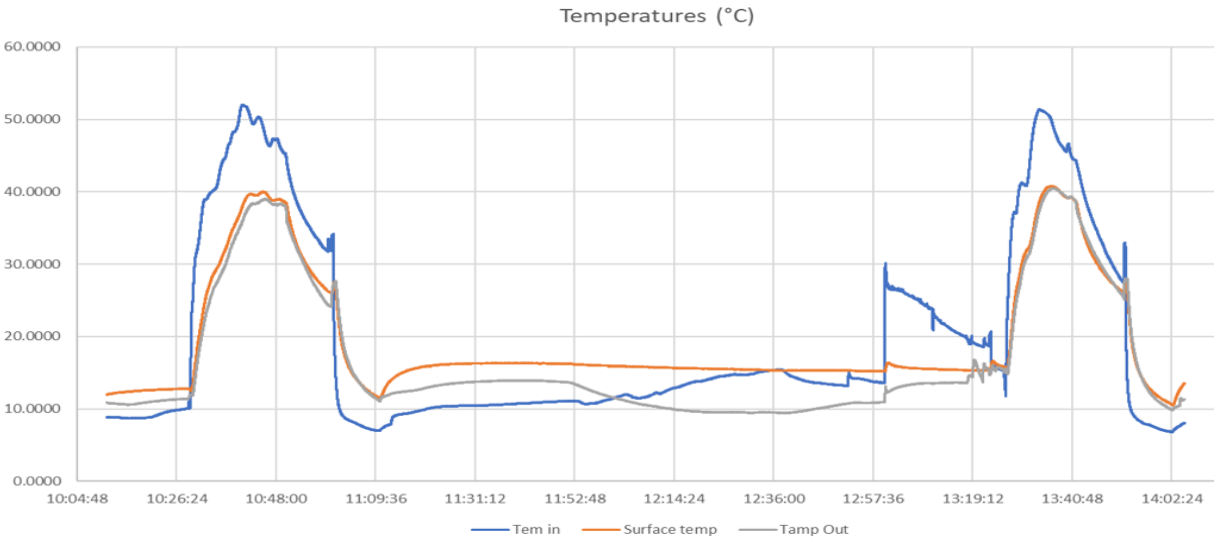

Time versus Temperature for section A2

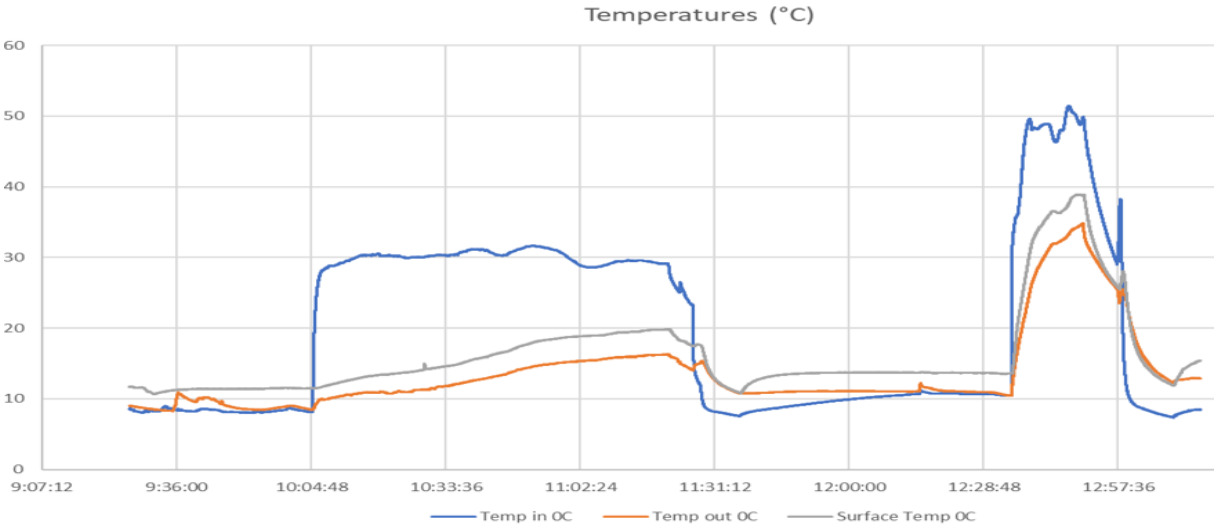

Experiment 1: Pressures recorded for section C6

Date	Time	Pressure in
26.02.2020	10:28	-0,091247
26.02.2020	10:30	4,762,892
26.02.2020	10:50	4,956,951
26.02.2020	10:58	-0,097840
26.02.2020	11:00	1,027,260
26.02.2020	11:06	5,182,658
26.02.2020	11:12	0,067728
26.02.2020	11:15	0,109268

Experiment 2: Pressures recorded for section C6

Date	Time	Pressure in
26.02.2020	13:00	0,061666
26.02.2020	13:03	6,551,334
26.02.2020	13:08	6,200,803
26.02.2020	13:25	-0,090205
26.02.2020	13:26	-0,012959
26.02.2020	13:27	3,308,357
26.02.2020	13:30	3,403,475
26.02.2020	13:41	3,522,119
26.02.2020	13:52	4,262,932
26.02.2020	14:02	4,167,333
26.02.2020	14:03	-0,098413

Experiment 1: Pressures recorded for section A2

Date	Time	Pressure in
27/02/20	10:04	-0.00308
27/02/20	10:05	0.245531
27/02/20	10:27	6.366907
27/02/20	10:34	6.779632
27/02/20	10:45	6.629474
27/02/20	10:47	6.931886
27/02/20	10:50	6.430291
27/02/20	10:55	6.259998
27/02/20	11:00	6.488234
27/02/20	11:05	6.347229
27/02/20	11:10	6.738869
27/02/20	11:15	6.773668
27/02/20	11:20	6.567423
27/02/20	11:25	0.002328
27/02/20	11:26	0.028605
27/02/20	11:28	6.689768
27/02/20	11:30	5.909529
27/02/20	11:36	5.739823
27/02/20	11:37	0.010463

Experiment 2: Pressures recorded for section A2

Date	Time	Pressure in
27/02/20	12:35	5.181573
27/02/20	12:36	5.088126
27/02/20	12:50	5.61725
27/02/20	12:51	0.044442
27/02/20	12:58	5.572312
27/02/20	12:59	5.86913
27/02/20	13:08	5.26744
27/02/20	13:09	5.790422

Calculations using Manning's Equation

Height(mm)	Height (ft)	Ɵ (radians)	Ɵ (degrees)	Area (ft^2)	Wetted P (ft)	Rh (ft)
1	0.00328084	0.271443707	15.5525788	0.00021136	0.288155105	0.002933973
1.5	0.00492126	0.332577237	19.055272	0.00038802	0.351605281	0.004414315
2	0.00656168	0.384175165	22.0116155	0.00059699	0.40448741	0.00590365
2.5	0.0082021	0.429686763	24.619238	0.00083374	0.45054385	0.00740205
3	0.00984252	0.470880348	26.9794566	0.00109521	0.491701497	0.008909583
3.5	0.01148294	0.508805991	29.1524359	0.00137917	0.529109487	0.010426319
4	0.01312336	0.544147619	31.177362	0.00168384	0.563519463	0.011952331
4.5	0.01476378	0.57738012	33.0814441	0.00200783	0.595455546	0.013487688
5	0.0164042	0.608849137	34.8844859	0.00234995	0.625300836	0.015032465
5.5	0.01804462	0.63881551	36.6014326	0.00270922	0.653345674	0.016586733
6	0.01968504	0.667481818	38.2438911	0.00308476	0.679816509	0.018150565
6.5	0.02132546	0.695009105	39.8210885	0.00347584	0.704894136	0.019724037
7	0.02296588	0.721527905	41.3405038	0.00388178	0.728725722	0.021307224
7.5	0.0246063	0.74714576	42.8082987	0.00430199	0.751433035	0.022900199
8	0.02624672	0.771952517	44.2296212	0.00473594	0.773118247	0.02450304
8.5	0.02788714	0.796024152	45.6088243	0.00518313	0.79386813	0.026115824
9	0.02952756	0.819425593	46.9496281	0.00564313	0.813757157	0.027738628
9.5	0.03116798	0.842212845	48.2552415	0.00611552	0.832849847	0.029371529
10	0.0328084	0.864434614	49.528455	0.00659993	0.851202557	0.031014608
10.5	0.03444882	0.886133575	50.7717139	0.00709601	0.868864881	0.032667943
11	0.03608924	0.907347367	51.9871747	0.00760343	0.885880749	0.034331615
11.5	0.03772966	0.928109387	53.1767508	0.00812189	0.902289316	0.036005705
12	0.03937008	0.948449427	54.3421493	0.00865111	0.918125665	0.037690294
12.5	0.0410105	0.968394203	55.4849008	0.00919081	0.933421391	0.039385465
13	0.04265092	0.987967775	56.6063838	0.00974075	0.948205079	0.041091301
13.5	0.04429134	1.007191904	57.7078453	0.01030068	0.962502697	0.042807885
14	0.04593176	1.026086351	58.7904173	0.01087038	0.976337929	0.044535303
14.5	0.04757218	1.044669122	59.8551317	0.01144963	0.989732456	0.04627364
15	0.0492126	1.062956678	60.9029315	0.01203823	1.002706188	0.048022981

Q estimated using a variation in "n"

cfs	ft3/min	L/min
0.000	0.0173361	0.4909018
0.001	0.041	1.174
0.001	0.077	2.177
0.002	0.124	3.509
0.003	0.183	5.177
0.004	0.254	7.187
0.006	0.337	9.542
0.007	0.432	12.244
0.009	0.540	15.295
0.011	0.660	18.695
0.013	0.793	22.446
0.016	0.937	26.546
0.018	1.095	30.995
0.021	1.273	36.033
0.024	1.460	41.351
0.028	1.662	47.053
0.031	1.877	53.141
0.035	2.105	59.617
0.039	2.348	66.484
0.043	2.604	73.741
0.048	2.874	81.390
0.053	3.158	89.432
0.058	3.456	97.868
0.063	3.768	106.700
0.068	4.094	115.927
0.074	4.434	125.551
0.080	4.788	135.572
0.086	5.156	145.990
0.092	5.538	156.807

Q estimated using no variation in "n"

cfs	ft3/m	L/min
6.35656E-06	0.000381	0.011
1.52074E-05	0.000912	0.026
2.81892E-05	0.001691	0.047894
0.000045437	0.002726	0.077198
0.000067042	0.004023	0.113905
0.000093068	0.005584	0.158123
0.000123560	0.007414	0.209929
0.000158548	0.009513	0.269374
0.000198051	0.011883	0.33649
0.000242081	0.014525	0.411298
0.000290642	0.017439	0.493803
0.000343733	0.020624	0.584006
0.000401350	0.024081	0.681897
0.000466587	0.027995	0.792734

0.000535438	0.032126	0.909714
0.000609271	0.036556	1.035155
0.000688108	0.041286	1.1691
0.000771970	0.046318	1.311584
0.000860878	0.051653	1.462639
0.000954847	0.057291	1.622293
0.001053894	0.063234	1.790574
0.001158031	0.069	1.968
0.001267272	0.076	2.153
0.001381627	0.083	2.347
0.001501108	0.090	2.550
0.001625722	0.098	2.762
0.001755480	0.105	2.983
0.001890387	0.113	3.212
0.002030451	0.122	3.450

“n” calculation for case #2 using Manning’s

h/D	n
0.004611	0.022338
0.006916	0.022507
0.009222	0.022676
0.011527	0.022845
0.013833	0.023014
0.016138	0.023183
0.018444	0.023353
0.020749	0.023522
0.023055	0.023691
0.02536	0.02386
0.027666	0.024029
0.029971	0.024198
0.032277	0.024367
0.034582	0.024373
0.036888	0.02446
0.039193	0.024547
0.041499	0.024634
0.043804	0.024721
0.04611	0.024808
0.048415	0.024895
0.050721	0.024981
0.053026	0.025068
0.055332	0.025155
0.057637	0.025242
0.059943	0.025329
0.062248	0.025416
0.064554	0.025503
0.066859	0.02559
0.069164	0.025677

Calculations using Darcy Equation

Channel Height	Sector angle	Sector area	Wetted perimeter	Hydraulic diameter	Flow rate A2 30°C	Flow rate C6 30°C
m	rad	m^2	m	m	l/min	l/min
0.001	0.272	0.000	0.088	0.001	0.094	0.128
0.0015	0.333	0.000	0.107	0.001	0.480	0.656
0.002	0.385	0.000	0.123	0.002	1.536	2.099
0.0025	0.430	0.000	0.137	0.002	3.796	5.187
0.003	0.472	0.000	0.150	0.003	7.967	10.889
0.0035	0.510	0.000	0.161	0.003	14.943	20.422
0.004	0.545	0.000	0.171	0.004	25.807	35.270
0.0045	0.578	0.000	0.181	0.004	41.850	57.195
0.005	0.610	0.000	0.190	0.005	64.578	88.256
0.0055	0.640	0.000	0.199	0.005	95.724	130.823
0.006	0.669	0.000	0.207	0.006	137.264	187.594
0.0065	0.696	0.000	0.214	0.006	191.424	261.613
0.007	0.723	0.000	0.222	0.006	260.698	356.287
0.0075	0.748	0.000	0.229	0.007	347.860	475.409
0.008	0.773	0.000	0.235	0.007	455.979	623.172
0.0085	0.797	0.000	0.242	0.008	588.434	804.194
0.009	0.821	0.001	0.248	0.008	748.929	1023.536
0.0095	0.844	0.001	0.253	0.009	941.510	1286.730
0.01	0.866	0.001	0.259	0.009	1170.582	1599.795
0.0105	0.888	0.001	0.264	0.010	1440.926	1969.266
0.011	0.909	0.001	0.270	0.010	1757.720	2402.217
0.0115	0.930	0.001	0.275	0.011	2126.552	2906.288
0.012	0.950	0.001	0.279	0.011	2553.448	3489.713
0.0125	0.970	0.001	0.284	0.012	3044.887	4161.345
0.013	0.990	0.001	0.288	0.013	3607.822	4930.691
0.0135	1.009	0.001	0.293	0.013	4249.708	5807.935
0.014	1.028	0.001	0.297	0.014	4978.519	6803.976
0.0145	1.046	0.001	0.301	0.014	5802.775	7930.459
0.015	1.065	0.001	0.305	0.015	6731.568	9199.809

Information about the sections C6 and A2

Information	Units	Data
Inner diameter of 9 5/8"	m	0.2168
Inner radius of 9 5/8"	m	0.1084
A2 total length	m	8.8
A2 inlet to outlet distance	m	8.2
A2 measured volume	l	0.85
C6 total length	m	8.28
C6 inlet to outlet distance	m	6
C6 measured volume	l	
Water visc. μ @ 10 C, 1bar	Pa s	0.00131
Water visc. @ 20 C	Pa s	0.001
Water visc. @ 30 C	Pa s	0.000797
Water visc. @ 40 C	Pa s	0.000653
Water visc. @ 50 C	Pa s	0.000547
No significant pressure dependency of viscosity		
Inlet pressure	bar	6.5
Inlet pressure	Pa	650000
Measured flow rate A2 Min	ml/(30 s)	235
	l/min	0.47
Measured flow rate A2 Max	ml/(30 s)	437.5
	l/min	0.875
Measured flow rate A2 after cold water	ml/(10 s)	661.6666667
	l/min	3.97
Measured flow rate C6 average	ml/(10 s)	840
	l/min	5.04
Measured flow rate C6 min	ml/(10 s)	680
	l/min	4.08
Measure flow rate C6 max	ml/(10 s)	1000
	l/min	6